

Differentiation and localization of target primitives using infrared sensors

Tayfun Aytaç and Billur Barshan

*Department of Electrical Engineering, Bilkent University
Bilkent, TR-06533 Ankara, Turkey
e-mail: {taytac, billur}@ee.bilkent.edu.tr*

Abstract

This study investigates the use of low-cost infrared sensors in the differentiation and localization of commonly encountered target primitives in indoor environments, such as planes, corners, edges, and cylinders. The intensity readings from such sensors are highly dependent on target location and properties in a way which cannot be represented in a simple manner, making the differentiation and localization process difficult. In this paper, we propose the use of angular intensity scans and present an algorithm to process them. This approach can determine the target type independent of its position. Once the target type is identified, its position can also be estimated. The method is verified experimentally. An average correct classification rate of 97% over all target types is achieved and targets are localized within absolute range and azimuth errors of 0.8 cm and 1.6°, respectively. The proposed method should facilitate the use of infrared sensors in mobile robot applications for differentiation and localization beyond their common usage as simple proximity sensors for object detection and collision avoidance.

1 Introduction

Infrared sensors are inexpensive, practical and widely available devices. However, it is often not possible to make reliable distance estimates based on the value of a single intensity return because the return depends on both the geometry and other properties of the reflecting target. Likewise, the properties of the target cannot be deduced from simple intensity returns without knowing its distance and angular location. In this paper, we propose a scanning technique and algorithm that can determine the type of the target in a manner which is invariant to its location. Once the target type is determined, its position (r, θ) can also be estimated. The method we propose is scalable in the sense that the accuracy can be increased by increasing the number of reference scans

without increasing the computational complexity of the differentiation and localization process.

Target differentiation and localization is of considerable interest in robotics applications, where there is need to identify targets and their positions in mobile robot environments for autonomous operation. Typical applications of infrared sensors in this area are mainly floor sensing, navigational referencing, and collision avoidance at short ranges [1]. In [2], a number of commercially available light-based sensors are evaluated for robotic space applications. In [3], infrared sensors are employed in locating edges of doorways where they are used in a complementary fashion with sonar sensors in mobile robot navigation. Other researchers have also fused information from infrared and ultrasonic sensors [4, 5]. In [6], system and implementation issues in infrared proximity sensing in robot manipulator motion planning are discussed. Following this work, [7] describes a teleoperated whole-sensitive robot arm manipulator whose whole body is covered with a sensitive infrared skin sensor to detect nearby objects. Processing the data from the artificial infrared skin by motion planning algorithms, real-time collision avoidance for the entire arm body is achieved in an unknown or dynamic environment. In another study [8], the properties of a planar surface at a known distance have been determined using the Phong illumination model, and using this information, the infrared sensor employed has been modeled as a range finder for surfaces at short distances. Reference [9] also deals with determining the range of a planar surface. Infrared sensors are used in door detection processes in [10]. However, to the best of our knowledge, no attempt has been made to differentiate and localize several kinds of targets using infrared sensors.

2 Target Differentiation & Localization

The infrared sensor [11] used in this study consists of an emitter and detector and works with 20–28 V DC

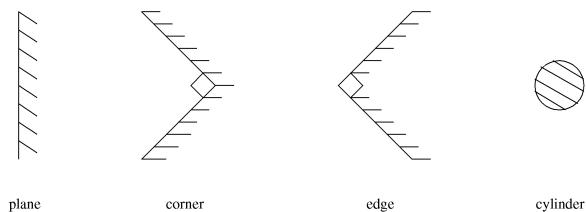


Figure 1: Target primitives used in this study.

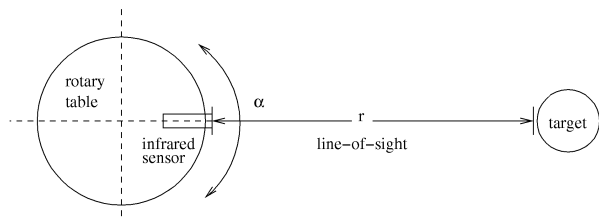


Figure 2: Top view of the experimental setup. The emitter and detector windows are circular with 8 mm diameter and center-to-center separation 12 mm. (The emitter is above the detector.) Both the scan angle α and the target azimuth θ are measured counter-clockwise from the horizontal axis.

input voltage, and provides analog output voltage proportional to the measured intensity. The detector window is covered with an infrared filter to minimize the effect of ambient light on the intensity measurements. Indeed, when the emitter is turned off, the detector reading is essentially zero. The sensitivity of the device can be adjusted with a potentiometer to set the operating range of the system.

The targets employed in this study are plane, 90° corner, 90° edge, and a cylinder of radius 4.8 cm, whose cross-sections are given in Figure 1. They are made of wood, each with a height of 120 cm. Our method is based on angularly scanning each target over a certain angular range. The infrared sensor is mounted on a 12 inch rotary table [12] (Figure 2) to obtain angular scans from these target primitives. The mean and standard deviation of 100 samples are calculated at each position of the rotary table to observe the effect of noise on the measurements. The standard deviation of the intensity measurements is about 0.1 V and is approximately constant with changing distance. Reference data sets are collected for each target with 2.5 cm distance increments, ranging from 15 cm to the maximum detectable range of each target, at $\theta = 0^\circ$. The output signal is processed using an 8-bit microprocessor compatible A/D converter chip having a conversion time of 100 μsec .

The resulting reference scans for plane, corner, edge

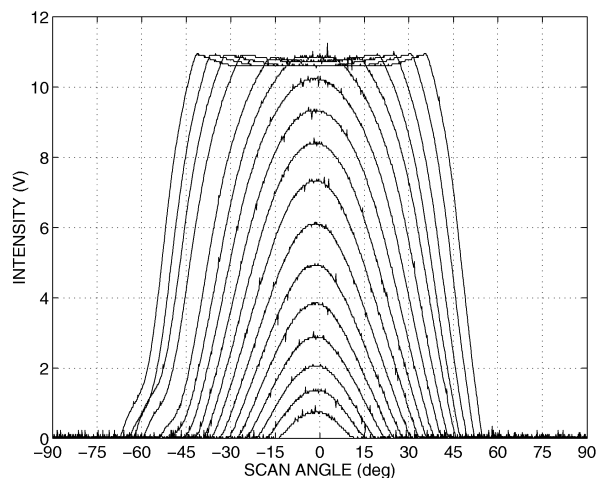


Figure 3: Intensity scans for planes at different distances.

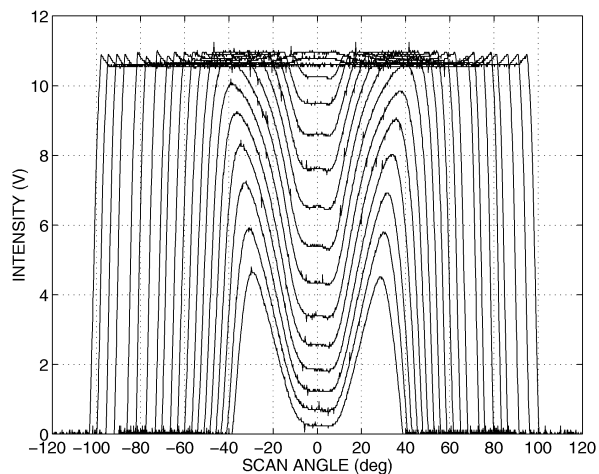


Figure 4: Intensity scans for corners at different distances.

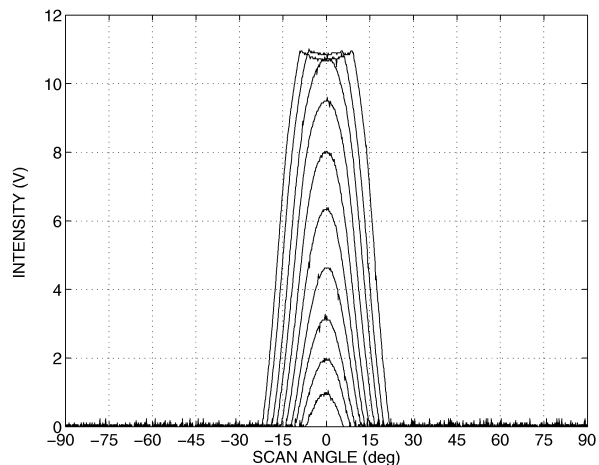


Figure 5: Intensity scans for edges at different distances.

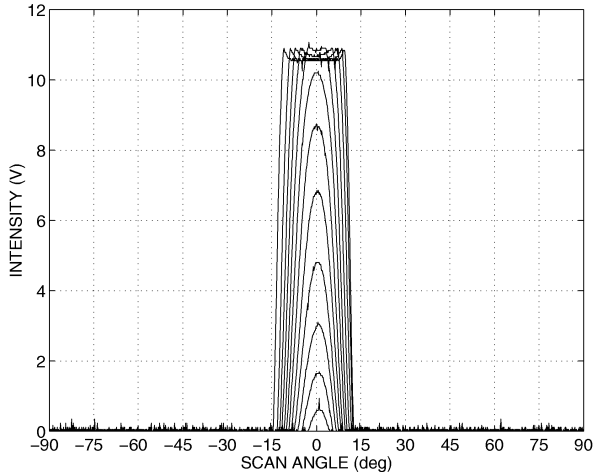


Figure 6: Intensity scans for cylinders at different distances.

and cylinder are shown in Figures 3–6, respectively. The intensity scans are θ -invariant but not r -invariant; changes in r do not result in any simple scaling. As we will see, these scans contain sufficient information to identify and localize the different target types with a good degree of accuracy. Figure 4 shows the distinctive double-humped scan pattern for the corner target (this double-humped pattern can be interpreted by thinking of the corner in terms of its two orthogonal constituent planes). As can be guessed from these figures, the greatest difficulty is encountered in differentiating cylinders and edges which have the most similar intensity patterns. Notice that the return signal intensities saturate at an intensity corresponding to 10.7 V output voltage.

We now describe how to determine the target type and position of an arbitrarily located target whose intensity scan has been observed. First, we check whether the observed scan $I(\alpha)$ exhibits saturation or not. This situation is treated separately as will be explained later in Section 2.3. A corner scan is considered saturated when its central intensity enters the saturation region, not the humps, since it is the former value which is critical for our method below.

We start by determining the target type. Unfortunately, direct comparison with the corresponding curves in Figures 3–6 is not possible since we do not yet know the distance of the target, and comparing with all the curves at all distances would be computationally very expensive. Therefore, we exploit the fact that the successive curves in Figures 3–6 exhibit a monotonic dependence on distance. Furthermore, when an observed scan is compared to the several successive curves in any of Figures 3–6, the two measures of difference between them described in Sections 2.1 and 2.2 also exhibit a monotonic fall

and rise around a single minimum. Therefore, we are assured that we will not be settling at a sub-optimal point if we compare the observed scan not with all scans at all distances but only with the four scans (one for each target type) whose central intensities are closest to that of the observed scan. (This can also be viewed as a kind of nearest-neighbour search.) Therefore, for unsaturated scans, only four comparisons need to be made. This remains the case even if the 2.5 cm increments are reduced to smaller values. This has the advantage that the accuracy of the system can be increased without increasing the cost of computation, which only depends on the number of angular samples (although a greater number of scans do have to be stored). As a test, we also ran a version of the method where *eight* comparisons were made using the scans with the nearest central intensities both above *and* below the observed central intensity, and also using *all* of the scans shown in Figures 3–6. These computationally more expensive approaches, exceedingly more so in the latter case, did not improve the result with respect to comparison with only four scans. In fact, in the matched filtering case discussed in Section 2.2, the results are even somewhat better when four scans are used, due to the fact that this systematic elimination of a priori suboptimal scans eliminates the small possibility that they will mistakenly be chosen as the best matching scan due to noise and other errors.

Two alternative approaches are employed in performing the four comparisons. These are discussed below in the following two subsections:

2.1 Least-Squares Approach

First, we estimate the angular position of the target as follows: Assuming the observed scan pattern is not saturated, we check if it has two humps or not. If so, it is a corner and we find the angular location of the dip in the middle of the two humps and the corresponding intensity value. If not, we find the angular location of the maximum and again the corresponding intensity value. These angular values can be directly taken as estimates of the angular position of the target. Alternatively, the angular position can be estimated by finding the center-of-gravity (COG) of the scan as follows:

$$\theta_{\text{COG}} = \frac{\sum_{i=1}^n \alpha_i I(\alpha_i)}{\sum_{i=1}^n I(\alpha_i)} \quad (1)$$

Ideally, these estimates would be equal, but in practice they differ by a small amount. We will consider the use of both alternatives when tabulating our results. From now on, we will refer to either estimate as the “center angle” of the scan.

Plots of the intensity at the center angle of each scan in Figures 3–6 as a function of the distance at which

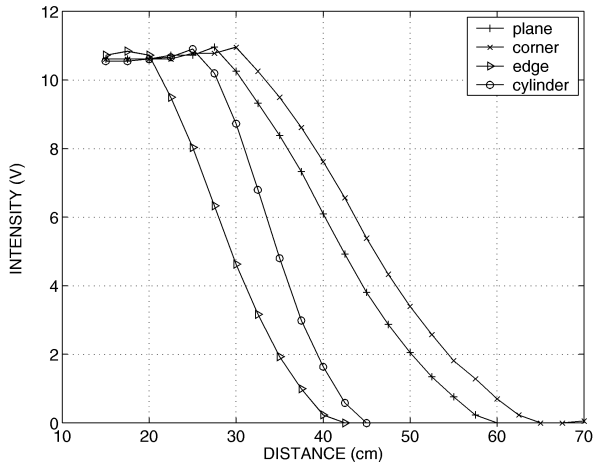


Figure 7: Central intensity versus distance curves for the different targets.

that scan was obtained, play an important part in our method. Figure 7 shows these plots for the maximum intensity (central dip intensity for corner) case.

In this approach, we compare the intensity scan of the observed target with the four reference scans by computing their least-squares differences after aligning their centers with each other. Since the squared difference is sensitive even to multiplicative factors which are close to unity, we have employed an interpolated reference scan obtained by linearly interpolating between the two consecutive scans whose central intensities are just above and just below the observed scan. The mean-square difference between the observed scan and the four interpolated scans, one for each possible target type, is computed as follows:

$$\mathcal{E}_j = \sum_{i=1}^n [I(\alpha_i - \alpha_{\text{align}}) - I_j(\alpha_i)]^2 \quad (2)$$

where I_j , $j = 1, 2, 3, 4$ denote the four interpolated scans. Here, α_{align} is the angular shift which is necessary to align both patterns. The target type resulting in the smallest value of \mathcal{E} is declared as the observed target. Once the target type is determined, the range can be estimated by using linear interpolation on Figure 7. Note that, this way, the accuracy of the method is not limited by the 2.5 cm spacing used in collecting the reference scans.

2.2 Matched Filtering Approach

As an alternative, we have also considered the use of matched filtering [13] to compare the observed and reference scans. The output of the matched filter is the cross-correlation between the observed intensity scan and the j th reference scan normalized by the

square root of its total energy:

$$y_j(l) = \frac{\sum_k I(\alpha_k) I_j(\alpha_{k-l})}{\sqrt{\sum_k [I_j(\alpha_k)]^2}} \quad (3)$$

The target type corresponding to the maximum cross-correlation peak is declared as the correct target type, and the angular position of the correlation peak directly provides an estimate of the azimuth angle of the target. Then, the distance is estimated by using linear interpolation on Figure 7 with the intensity value at the azimuth estimate.

2.3 Saturated Scans

If saturation is detected in the observed scan, special treatment is necessary. In the least-squares approach, mean-square difference between the aligned observed scan and *all* the saturated reference scans are computed and the target type with the minimum mean-square difference is chosen. The range estimate of the target is taken as the distance corresponding to the scan resulting in the minimum mean-square difference. Similarly, for the matched filter, correlation between the observed scan and *all* the stored saturated reference scans is computed and the target resulting in the highest correlation peak is selected. The range estimate is again taken as that of the best matching scan.

It should be noted that, in the saturated case, range estimation accuracy is limited by the 2.5 cm interval at which the reference scans were taken since interpolation is not possible. If this accuracy is not satisfactory, it can be improved by reducing the 2.5 cm intervals. We underline that the 2.5 cm interval does not limit the range estimation accuracy in the unsaturated case, where accurate interpolation is possible from Figure 7.

3 Experimental Verification and Discussion

In this section, we experimentally verify the proposed method by locating the targets at randomly selected distances and azimuth angles (r, θ) and collecting a total of 120 test scans. The targets are randomly located at azimuths varying from -45° to 45° from 15 cm up to the maximum ranges in Figures 3–6.

The results of least-squares based target differentiation are displayed in Tables 1 and 2 in the form of target confusion matrices. Table 1 gives the results obtained using the maximum (or the central dip for corner) intensity values, and Table 2 gives those obtained using the intensity value at the COG of the scans. The average accuracy over all target types can be found by summing the correct decisions given along the diagonal of the confusion matrix and dividing this sum by the total number of test trials

(120). The average correct classification rates obtained by using the max/dip and the COG variations of the least-squares approach are 93% and 89%, respectively.

Matched filter differentiation results are presented in Table 3. The average accuracy of differentiation over all target types is 97% which is better than that obtained with the least-squares approach. The matched filter correctly classifies planar targets as well as corners with an accuracy of 100%.

Table 1: Target confusion matrix: least-squares based classification (max/dip variation) (P: plane, C: corner, E: edge, CY: cylinder).

target	differentiation result				total
	P	C	E	CY	
P	29	–	1	–	30
C	–	30	–	–	30
E	1	–	26	3	30
CY	4	–	–	26	30
total	34	30	27	29	120

Table 2: Target confusion matrix: least-squares based classification (COG variation).

target	differentiation result				total
	P	C	E	CY	
P	30	–	–	–	30
C	–	30	–	–	30
E	5	–	23	2	30
CY	4	–	2	24	30
total	39	30	25	26	120

Table 3: Target confusion matrix: matched filter based classification.

target	differentiation result				total
	P	C	E	CY	
P	30	–	–	–	30
C	–	30	–	–	30
E	–	–	29	1	30
CY	–	–	3	27	30
total	30	30	32	28	120

As shown in the tables, corners are always correctly identified regardless of which method is used, due to their distinctive signature. Second best to corners are planes which are also usually correctly identified. Cylinders and edges are the most confused target types as we had expected from the similar nature of their intensity scans. Nearly all misclassified targets are located at far ranges where the return signal intensities are very weak.

The average absolute range and azimuth estimation errors for the different approaches are presented in

Table 4: Absolute range and azimuth estimation errors over all test targets.

method		P	C	E	CY	ave. error
least squares (max/dip)	$r(\text{cm})$	1.0	0.7	1.1	1.8	1.2
	$\theta(\text{deg})$	4.1	5.7	2.3	1.7	3.5
least squares (COG)	$r(\text{cm})$	0.5	0.7	4.3	1.5	1.7
	$\theta(\text{deg})$	2.9	2.8	3.0	2.4	2.8
matched filter	$r(\text{cm})$	0.7	0.7	0.8	1.0	0.8
	$\theta(\text{deg})$	1.2	1.7	1.8	1.8	1.6

Table 4. As seen in the table, using the max/dip and COG variations of the least-squares approach, the target ranges are estimated with average absolute range errors of 1.2 cm and 1.7 cm, respectively. Matched filtering results in an average absolute range error of 0.8 cm which is much better than that obtained with the least-squares approach. The greatest contribution to the range errors comes from targets which are incorrectly differentiated. If we average over only correctly differentiated targets, the average absolute range errors are reduced to 0.6 cm, 0.6 cm, and 0.7 cm for the max/dip and COG variations of least-squares and the matched filter approaches, respectively. Since these numbers are comparable, we may conclude that the superior range accuracy of matched filtering is mostly a consequence of its superior differentiation accuracy.

As for azimuth estimation, matched filtering results in an average absolute estimation error of 1.6° , which is the best among the different approaches compared. Averaging the azimuth errors over only correctly differentiated targets does not result in significant changes. This is due to the fact that azimuth estimation is not dependent on correct differentiation.

Because of the sharpness of the scans for the cylindrical target around their peaks, azimuth estimation of cylinders is more accurate than that of other targets when the least-squares approach is used. On the other hand, angular localization of corners is less accurate since it is difficult to estimate with good accuracy the exact angular location of the relatively shallow central dip, especially with the max/dip variation of least-squares approach. The COG variation is, on the average, better than the max/dip variation in azimuth estimation due to the fact that COG based calculations average out the noise in the return signal intensities.

4 Conclusion

In this study, differentiation and localization of commonly encountered indoor features or targets such as plane, corner, edge, and cylinder is achieved using an

inexpensive infrared emitter and detector pair. Different approaches are compared in terms of correct target differentiation, and range and azimuth estimation accuracy. A typical application of the demonstrated system would be in mobile robotics in surveying an unknown environment composed of such features or targets. Many artificial environments fall into this category. We plan to test and evaluate the developed system on a small mobile robot in our laboratory for map building in a test room composed of the primitive target types considered in this study.

The accomplishment of this study is that even though the intensity patterns are highly dependent on target location, and this dependence cannot be represented by a simple relationship, we achieve position-invariant target differentiation. An average correct target differentiation rate of 97% over all target types is achieved and targets are localized within absolute range and azimuth errors of 0.8 cm and 1.6°, respectively. The method we propose is scalable in the sense that the accuracy can be increased by increasing the number of reference scans without increasing the computational cost.

In this paper, we have demonstrated target differentiation using four basic target types. However, based on the data we have collected, it seems possible to increase this number up to at least ten, provided the targets are not too similar. Current work investigates the deduction of not only the geometry but also the surface properties of the target from its intensity scan without knowing its location. Preliminary results indicate that the method of this paper can be applied to this case with little or no modification by treating the combination of a particular geometry and particular surface as a generalized target type. These results will be reported elsewhere [14]. Future work may involve developing parametric models for the curves in Figures 3–6 which would enable more direct determination of the target type and position.

5 Acknowledgment

This research was supported by TÜBİTAK under BDP and 197E051 grants. The authors would like to thank the Robotics Research Group of the University of Oxford for donating the infrared sensors.

References

- [1] H. R. Everett, *Sensors for Mobile Robots, Theory and Application*. 289 Linden St., Wellesley, MA: A K Peters, Ltd., 1995.
- [2] L. Korba, S. Elgazzar, and T. Welch, “Active infrared sensors for mobile robots,” *IEEE Trans. Instrum. Meas.*, vol. 43, no. 2, pp. 283–287, April 1994.
- [3] A. M. Flynn, “Combining sonar and infrared sensors for mobile robot navigation,” *Int. J. Robot. Res.*, vol. 7, no. 6, pp. 5–14, December 1988.
- [4] A. M. Sabatini, V. Genovese, E. Guglielmelli, A. Mantuano, G. Ratti, and P. Dario, “A low-cost, composite sensor array combining ultrasonic and infrared proximity sensors,” in *Proc. IEEE/RSJ Int. Conf. Intell. Robots Syst.*, pp. 120–126, Pittsburgh, Pennsylvania, U.S.A., 5–9 August 1995.
- [5] H. M. Barbera, A. G. Skarmeta, M. Z. Izquierdo, and J. B. Blaya, “Neural networks for sonar and infrared sensors fusion,” in *Proc. Third Int. Conf. Information Fusion*, vol. 7, pp. 18–25, France, July 2000.
- [6] E. Cheung and V. J. Lumelsky, “Proximity sensing in robot manipulator motion planning: system and implementation issues,” *IEEE Trans. Robot. Automat.*, vol. 5, no. 6, pp. 740–751, December 1989.
- [7] V. J. Lumelsky and E. Cheung, “Real-time collision avoidance in teleoperated whole-sensitive robot arm manipulators,” *IEEE Trans. Syst., Man, Cybern.*, vol. 23, no. 1, pp. 194–203, January/February 1993.
- [8] P. M. Novotny and N. J. Ferrier, “Using infrared sensors and the Phong illumination model to measure distances,” in *Proc. IEEE Int. Conf. Robot. Automat.*, pp. 1644–1649, Detroit, MI, 2 April 1999.
- [9] B. Ando and S. Graziani, “A new IR displacement system based on noise added theory,” in *Proc. IEEE Instrum. Meas. Tech. Conf.*, pp. 482–485, Budapest, Hungary, 21–23 May 2001.
- [10] G. Beccari, S. Caselli, and F. Zanichelli, “Qualitative spatial representations from task-oriented perception and exploratory behaviors,” *Robot. Autonom. Syst.*, vol. 25, no. 3/4, pp. 147–157, 30 November 1998.
- [11] *IRS-U-4A Datasheet*, Matrix Elektronik, AG, Kirchweg 24 CH-5422 Oberehrendingen, Switzerland.
- [12] *RT-12 Rotary Positioning Table*, Arrick Robotics, P.O. Box 1574, Hurst, Texas, 76053, URL: www.robotics.com/rt12.html, 2002.
- [13] J. W. Goodman, *Introduction to Fourier Optics*, 2nd ed., McGraw-Hill, New York, 1996, pp. 246–249.
- [14] T. Aytaç, *Differentiation and Localization of Target Primitives Using Infrared Sensors*, M.Sc. thesis, Bilkent University, Department of Electrical Engineering, Ankara, Turkey, July 2002.